Natural Convection of Liquid Metals in Vertical Cavities

F. Wolff
Research Assistant

C. Beckermann
Research Assistant

R. Viskanta
Professor
Heat Transfer Laboratory,
School of Mechanical Engineering,
Purdue University, West Lafayette, Indiana

■A combined experimental and numerical study is reported of natural convection heat transfer and fluid flow in vertical cavities filled with liquid metals. Experiments are performed in two different test cells with two opposing side walls held at constant but different temperatures and the remaining walls well insulated. Tin and gallium are used as the fluids inside these cavities. Temperature measurements are employed to deduce the significance of natural convection in the liquid metals as well as to verify the results of numerical simulations of the experiments. The flow structure is visualized by the predicted streamlines. For various values of the governing dimensionless parameters, it is found that the natural convection patterns in liquid metals are considerably different from those found in fluids of high Prandtl number. The flow is characterized by a large convection cell in the center and small recirculation cells in the corners of the cavity. The heat fluxes at the hot and cold vertical walls show a variation reflecting the complicated flow patterns. The need for highly accurate three-dimensional numerical simulations is emphasized.

Keywords: *conduction, enclosure flows, liquid metals, measurement techniques, moving boundaries, natural convection, numerical methods, phase-change phenomena*

INTRODUCTION

Thermally driven flow in rectangular cavities with uniform but different temperatures imposed at two opposite side walls has been studied both experimentally and numerically. Comprehensive reviews of natural convection in such enclosures are available [1, 2]. Geophysical systems, nuclear reactor safety, casting of metals, and metals processing are just a few applications motivating research in this area.

However, little experimental and theoretical work has been conducted with liquid metals as the fluid occupying the vertical enclosure [3]. It is now generally accepted that the results obtained for ordinary nonmetallic fluids (ie, fluids with a high Prandtl number) cannot be applied to liquid metals having a Prandtl number well below unity [4]. This is mainly due to the important role played by fluid inertia and thermal conductivity during natural convection of a liquid metal.

The effect of buoyancy-induced flow on the temperature distribution and heat transfer in a rectangular enclosure filled with tin has been investigated both numerically and experimentally [4, 5]. Because of the small depth (0.32–0.95 cm) of the test cell used in the experiments [4], the two-dimensional model [5] overpredicts the intensity of the natural convection flow and heat transfer. A comparison between temperature measurements and the results of a three-dimensional model show similar overpredictions for natural convection of liquid gallium [6]. These discrepancies have been attributed to measurement errors, heat losses from the test cell, and inaccuracies in the numerical results. Heat transfer measurements in a vertical test cell filled with liquid tin have conclusively shown that models based on pure heat conduction are not adequate, although metals have a very high thermal conductivity [7]. Numerical simulations of natural convection of liquid metals in narrow cavities (ie, with a high aspect ratio) have revealed the existence of complicated flow structures, including multiple convection cells [8].

As evident from the above review of the literature, natural convection of low Prandtl number fluids has not received adequate research attention. Hence, it is the purpose of the present paper to investigate the flow and heat transfer in a rectangular cavity filled with a liquid metal. The two vertical side walls are held at constant but different temperatures, while the connecting horizontal top and bottom walls are considered adiabatic. Experiments are performed in two different test cells using tin as the fluid in one and gallium in the other. These metals are selected as the working fluids because their thermophysical properties are reasonably well documented [9, 10] and their fusion temperature is low in comparison to other metals (gallium, 29.78°C; tin, 231.9°C). In particular, the experiments with gallium can be conducted close to the ambient temperature, reducing the need for extensive insulation of the top and bottom walls. It should also be noted that the Prandtl numbers of tin and gallium differ by more than a factor of 2 near their respective fusion temperatures ($Pr \approx 0.011$ for tin and $Pr \approx 0.028$ for gallium). Temperature measurements are employed to deduce the significance of natural convection in the liquid metals as well as to verify the results of numerical simulations of the experiments. The corresponding streamlines

Address correspondence to Professor Raymond Viskanta, School of Mechanical Engineering, Purdue University, West Lafayette, IN 47907.

Experimental Thermal and Fluid Science 1988; 1:83–91

0894-1777/88/$3.50

Table 1. Summary of Experimental Conditions

Experiment	*Fluid*	$T_H - T_C$ (°C)	*A*	*Pr*	*Ra*
1	Tin	2.5	1.0	0.011	3.659×10^5
2	Tin	2.5	0.75	0.011	3.659×10^5
3	Gallium	5.0	1.0	0.0208	1.682×10^5
4	Gallium	20.0	1.0	0.0208	6.727×10^5

predicted by the numerical model serve to visualize the complicated structure of the flow field. By using different fluids, test cells, and temperature differences of the side walls, it has been possible to perform experiments for certain ranges of the governing parameters (ie, Ra, Pr, and A, the aspect ratio).

EXPERIMENTS

The two different setups used for the experiments with tin and gallium are described separately in the following sections. A number of natural convection experiments were performed. The values of the dimensionless parameters of the four experiments selected for comparison with the numerical predictions are summarized in Table 1. All properties were evaluated at a temperature of $(T_H + T_C)/2$.

Tin

The experiments with tin were performed in a rectangular cavity with two vertical side walls at constant but different temperatures. The remaining walls of the cavity were well insulated. Figure 1*a* shows the principal design features of the experimental apparatus. The test cell was constructed from a commercially available five-sided Pyrex glass tank with walls 7 mm thick. Since the vertical extent of the tank was larger than the desired height of the test section, the bottom of the tank was partially filled with sand. A Pyrex glass plate 5 mm thick was placed on the sand to separate the test region from the sand. Two heat exchangers, which served as the heat source/sink, were then inserted into the tank and fixed on two opposite vertical walls. The glass plate at the bottom, two vertical walls of the glass tank, and the two heat exchangers formed the bottom and side walls respectively, of the test section. A 5 mm thick lava plate, serving as the top boundary of the test region, was placed on the tin. Another 75 mm thick lava plate was situated on top of each heat exchanger. Between the two lava plates was an air gap whose thickness varied with the aspect ratio. The configuration allowed flexibility to vary the aspect ratio and provided good insulation at the top. Slots were milled into both lava plates to enable insertion of probes from the top.

The actual test region was 8.89 cm wide and 12.6 cm deep. The height was 6.66 or 8.89 cm depending on the desired aspect ratio (0.75 or 1.0). The entire glass tank was inserted into a wooden box that was 8 cm larger than the tank on all four sides and at the bottom. The space between the box and the glass tank was filled with Sylox 2 micron-sized silica, an extremely good insulator (k = 0.02 W/mK).

Each of the two heat exchanges consisted of a 10 mm thick copper plate and five electric resistance heaters. The copper plate was in direct contact with the test material. The heaters were attached to the back of the copper plate. Each heater (Fig. 1*b*) was made out of two 2.54 mm thick high thermal conductivity boron nitride plates (k = 65 W/mK) and a 0.35 mm diameter nickel-

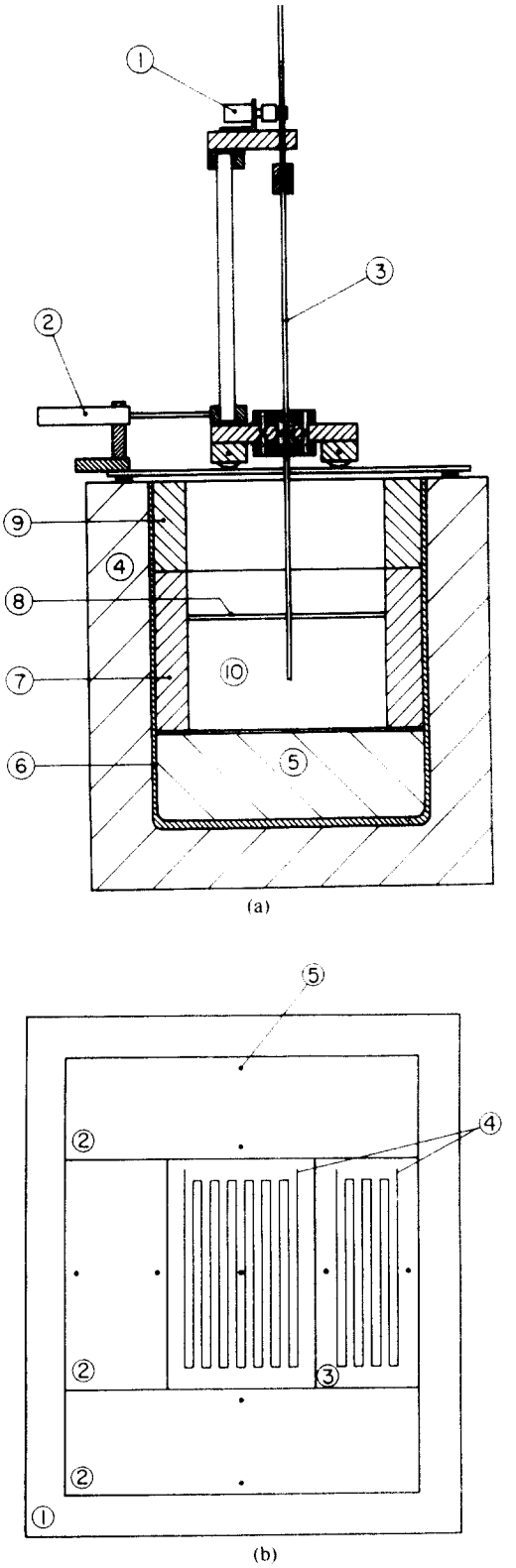

Figure 1. (*a*) Schematic of the apparatus for experiments with tin. 1, ten-turn potentiometer; 2, linear potentiometer; 3, probe; 4, Sylox 2 micron sized silica; 5, sand; 6, five-side glass tank; 7, heat exchangers; 8, 75 mm lava plate; 9, 5 mm lava plate; 10, tin. (*b*) Schematic diagram of the heat exchangers. 1, copper block; 2, heater (assembled); 3, grooved boron nitride plate (top plate of the heater removed); 4, nickel-chromium wire; 5, thermocouple locations.

chromium wire having an electrical resistivity of 9.6 ohms/m. In the plate that was in direct contact with the copper plate, 0.5-mm deep grooves were milled. The nickel-chromium wire was laid into the grooves, and the other boron nitride plate was placed on top of the grooved plate. The temperature of each heater was measured with either one or two type-K thermocouples, which were located in the copper plate at a distance of 0.02 mm from the surface adjacent to the tin. A Hewlett-Packard Model 3852 data logger was used to control the electric power input into the heaters so as to achieve a uniform temperature over the entire copper plate. This was accomplished by comparing the temperatures measured at the copper surface with the temperature desired as the boundary condition. Based on this comparison, the relay of each individual heater was either opened or closed. Due to heat losses from the back of the heat exchangers, it was sufficient to regulate the electric power input to keep the hot and cold walls at the desired temperature. With this heat exchanger design and the relatively small temperature differences between the heat exchangers in the experiments with tin, the temperature nonuniformities along the copper plate were reduced to 0.1°C.

Temperatures in the liquid tin were measured with a movable thermocouple probe. In order to determine the location of the probe, an x-y measurement system was developed that consisted of a rectangular frame and a cart. The frame, fixed on top of the wooden box, had rails on two opposite sides that served as guideways for the wheels of the cart. The position of the cart and thus the horizontal location of the probe was determined with a linear potentiometer attached to the cart and fixed to the frame. The vertical position of the probe was measured with a ten-turn potentiometer that was installed on the cart. A gear on the shaft of the ten-turn potentiometer gripped a precision rack connected to the probe. When the probe was moved up and down, the rack induced a rotation at the ten-turn potentiometer. The resulting electrical signals from the potentiometers were fed into the data logger. It was estimated that the position of the probe could be determined with an accuracy of ±1 mm.

The temperature probe consisted of a type K thermocouple wire inserted into a 3 mm O.D. glass tube. For protection purposes, the thermocouple bead at the tip of the rod was coated with a thin layer of high thermal conductivity epoxy. The thermocouple was calibrated against the freezing point of tin with an accuracy of ±0.1°C. The temperatures in the tin were measured at the vertical center plane at heights of $\eta = 0.1$, 0.5, and 0.9 measured from the bottom of the test section. The probe was traversed horizontally through the liquid, against the assumed direction of the flow, in order to minimize the disturbance of the flow and temperature fields by the previous measurements. At each location, the reading of the thermocouple was checked several times to ensure steady-state conditions at the instant of data acquisition. The test material used in this experimental apparatus was 99.99% pure tin with a melting point of 231.9°C. The thermophysical properties of liquid tin were obtained from the literature [9, 10].

Gallium

The experiments with liquid gallium were performed in a well-insulated test cell of square cross section. The test cell had inside dimensions of 4.76 cm in height and width and 3.81 cm in depth. The horizontal top and bottom walls were constructed of phenolic plates, while the vertical front and back walls were made of Plexiglas. The two vertical side walls, which served as the heat source/sink, were multipass counterflow heat exchangers machined out of a copper plate. Each heat exchanger was connected to a constant-temperature bath (Haake A85) so that the vertical side walls could be maintained at different temperatures. The temperature of each copper heat exchanger was measured at three locations with three thermocouples epoxied separately into small-diameter holes drilled close to the surface of the copper plate facing the gallium.

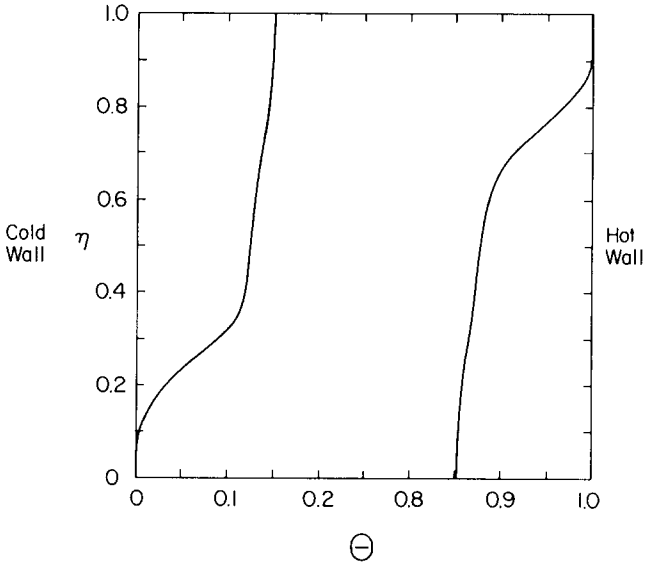

Figure 2. Typical temperature profiles of the hot and cold heat exchangers during the experiments with gallium.

In the experiments, considerable problems were encountered with the uniformity of the heat exchanger temperatures. This can be attributed to strong variations in the local heat fluxes in the vertical direction. The surface temperatures of the heat exchangers varied by up to 15% of the maximum temperature different ($T_H - T_C$) across the test cell. Typical surface-temperature variations of the hot and cold heat exchangers are shown in Fig. 2. Additional measurements indicated that, as expected, the temperatures were relatively uniform in the horizontal direction. In the numerical simulation of the experiments with gallium (refer to the following section), the *measured* temperature distributions of the heat exchangers were used as the boundary conditions at the vertical side walls (instead of $\Theta = 0.1$ at $\xi = 0.1$; $0 < \eta < A$). This procedure results in more realistic boundary conditions and thus better agreement between the measured and predicted temperatures.

Measurement of the temperature distribution inside the test cell was made with 33 thermocouples (type T) with a wire diameter of 0.127 mm. They were placed in three stainless steel rakes that were located at heights of $\eta = 0.133$, 0.5, and 0.867 measured from the bottom of the test cell. The rakes were positioned such that the temperatures were measured along the vertical center place of the test cell. The uncertainty in the location of each thermocouple bead was approximately ±0.2 mm. All thermocouples were calibrated with an accuracy of ±0.1°C. The gallium used in the experiments had a purity of 99.99% and a fusion temperature of 29.78°C. The thermophysical properties of gallium were obtained from the literature [10].

ANALYSIS

Governing Equations

A schematic of the physical model and coordinate system is shown in Fig. 3. It is assumed that the flow is steady, laminar,

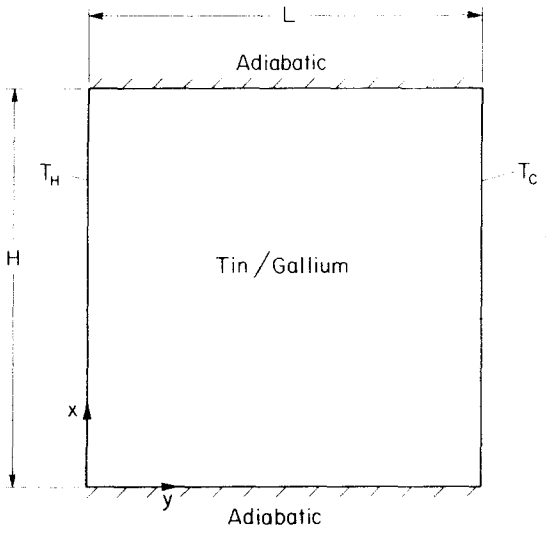

Figure 3. Schematic of the physical model and coordinate system.

incompressible, and two-dimensional. The thermophysical properties of the fluid are assumed constant, except for the density in the buoyancy term in the momentum equations. In terms of dimensionless variables (see Nomenclature), the conservation equations for mass, momentum, and energy can be written, respectively, as

$$\nabla \cdot \mathbf{u} = 0 \tag{1}$$

$$(\mathbf{u} \cdot \nabla)\mathbf{u} = -\nabla P + \mathrm{Pr}\,\nabla^2\mathbf{u} + \mathrm{Ra}\,\mathrm{Pr}\,\Theta\mathbf{e}_\eta \tag{2}$$

$$\mathbf{u} \cdot \nabla\Theta = \nabla^2\Theta. \tag{3}$$

The boundary conditions are given in dimensionless form as

$$\begin{aligned} &\Theta = 1, \quad \mathbf{u} = 0 \quad \text{at } \xi = 0,\ 0 \le \eta \le A \\ &\Theta = 0, \quad \mathbf{u} = 0 \quad \text{at } \xi = 1,\ 0 \le \eta \le A \\ &\frac{\partial\Theta}{\partial\eta} = 0, \quad \mathbf{u} = 0 \quad \text{at } \eta = 0,\ 0 \le \xi \le 1 \\ &\frac{\partial\Theta}{\partial\eta} = 0, \quad \mathbf{u} = 0 \quad \text{at } \eta = A,\ 0 \le \xi \le 1. \end{aligned} \tag{4}$$

The results for the local heat fluxes at the hot and cold walls are presented in terms of the local Nusselt number, defined as

$$\mathrm{Nu} = \frac{hL}{k} = -\frac{\partial\Theta}{\partial\xi}\bigg|_{\substack{\xi=0 \\ \xi=1}}. \tag{5}$$

Numerical Procedures

The governing equations, Eqs. (1)–(4), were solved utilizing the SIMPLER algorithm [11]. This algorithm is based on a control-volume formulation. The combined convective and diffusive fluxes across the control surfaces are discretized using the power-law scheme. The solution of the discretization equations was obtained iteratively using the tridiagonal matrix algorithm.

The mesh size required for sufficient numerical accuracy depended mainly on the Rayleigh (Ra) and Prandtl (Pr) numbers. In the simulations of the experiments (refer to the following section), a grid of 50 × 50 nodal points was employed. The nodal points were distributed using a power-law clustering scheme such that the grid distribution was symmetric about $\xi = 1/2$ and $\eta = A/2$. This procedure resulted in a greater concentration of points near the vertical and horizontal boundaries, where the velocity and temperature gradients are largest. It is realized that the present number of nodal points might not be sufficient to obtain accurate results for the velocities and temperatures in all regions of the computational domain. However, it is believed that the structures of the flow and heat transfer (ie, recirculation cells, boundary layers, etc) were resolved with sufficient detail.

The iterations were terminated when the dependent variables agreed to four significant digits at each nodal point and the residual source of mass was less than 10^{-6}. Convergence of the numerical solution was also checked by comparing the Nusselt numbers obtained along the two vertical side walls. The agreement between the average values was always better than 0.01%. The calculations were performed on a CYBER 205 computer. Due to an extremely slow rate of convergence, the computations required up to 1500 CPU seconds. Extensive tests of the accuracy of the numerical algorithm were performed [12], and excellent agreement with benchmark solutions reported in the literature (for natural convection of air) was found.

RESULTS AND DISCUSSION

Flow Structure

Figures 4*a*, 5*a*, 6*a*, and 7*a* show the streamlines for the simulations of experiments 1–4, respectively. In order to illustrate important details of the flow structure, the increments between the streamlines were chosen not to be equal. Consequently, the spacings between the streamlines represent different magnitudes of the mass flow rate.

The streamlines of all four simulations (Figs. 4*a*–7*a*) show a large concentric, clockwise-rotating convection cell. In the center of this convection cell, the velocities are as much as one order of magnitude lower than the ones in the boundary layers. Interestingly, there exist small recirculation cells in all four corners of the enclosure. At these locations, the main flow separates from the side walls and makes a 90° turn. Since the velocities of the fluid in the boundary layers near the hot and cold walls are higher than the velocities along the horizontal top and bottom walls, the separation of the flow occurs earlier in the upper right and lower left corners than in the lower right and upper left corners. Accordingly, larger recirculation regions are observed in the top right and bottom left corners than in the other two corner locations. It can also be seen that the larger recirculation regions comprise two small convection cells, while there is only one eddy in the upper left and lower right corners. Owing to the secondary recirculation cells, the impingement of the main flow on all four walls of the enclosures does not occur in the immediate vicinity of the corners, as would be expected in natural convection of a high Prandtl number fluid in the same Rayleigh number range [2], but is vertically and horizontally shifted at the side walls and at the top and bottom walls, respectively.

A comparison of Figs. 4*a* and 5*a* demonstrates the change of the flow structure due to a different aspect ratio. For $A = 1.0$ (Fig. 4*a*) the flow is slightly stronger, resulting in a thinner velocity boundary layer and in smaller secondary recirculation cells than for $A = 0.75$ (Fig. 5*a*). Figures 6*a* and 7*a* show the streamlines corresponding to the simulation of the experiments with gallium. Because of the temperature nonuniformities along the hot and cold walls (refer to the experimental setup for gallium), the flow field

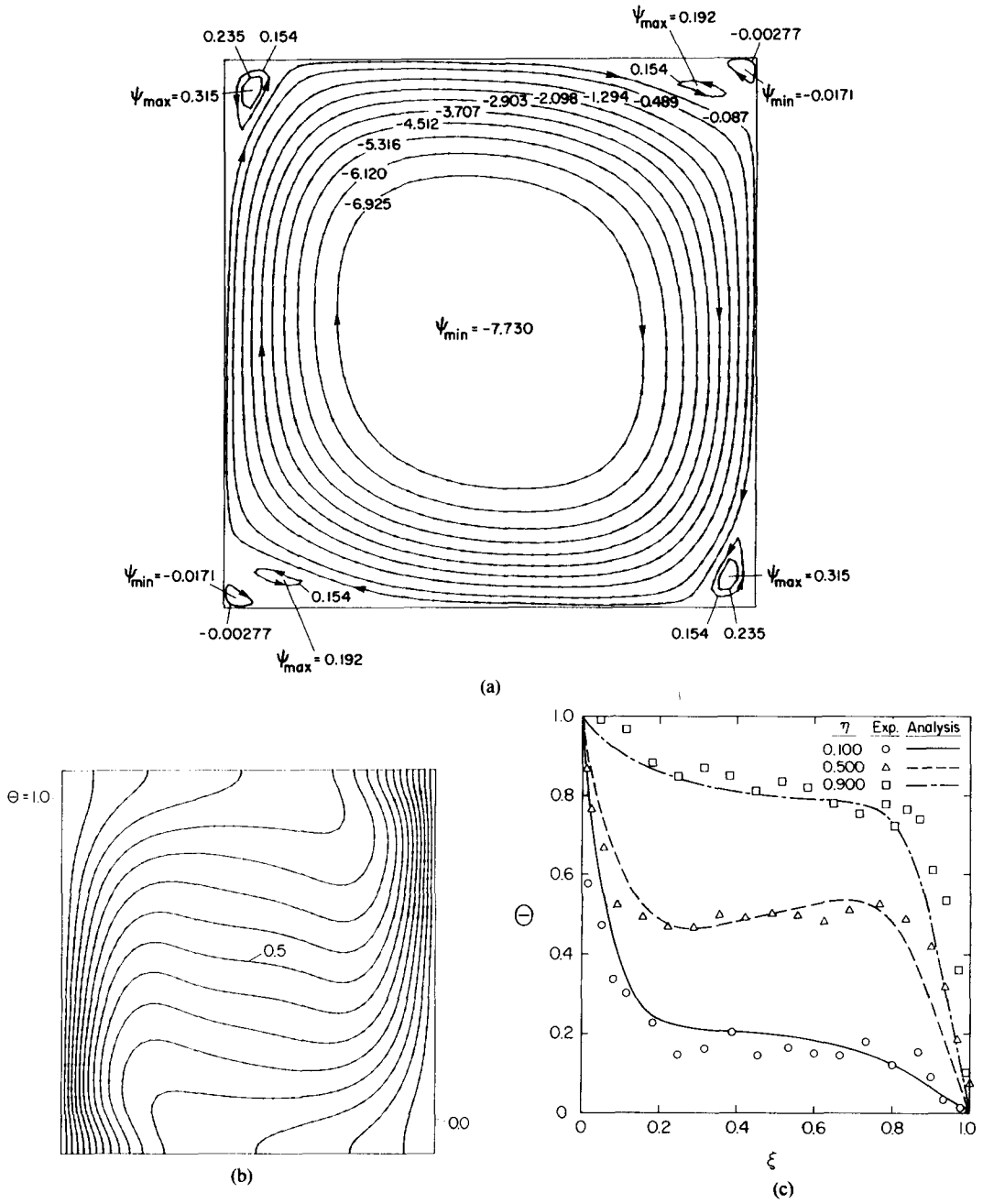

Figure 4. Measured and predicted results for experiment 1. (*a*) Streamlines; (*b*) isotherms (equal increments); (*c*) temperature profiles.

is not truly symmetric about the diagonals of the cavity, as observed for natural convection in an enclosure with constant-temperature boundary conditions. The influence of the Rayleigh number on the flow pattern can be deduced by comparing Fig. 6*a* (Ra = 1.682×10^5) and Fig. 7*a* (Ra = 6.727×10^5). Due to a higher Rayleigh number in experiment 4 (Fig. 7*a*), the secondary convection cells are smaller and the hydrodynamic boundary layers are thinner than in experiment 3 (Fig. 6*a*).

Heat Transfer Characteristics

The predicted isotherms for experiments 1–4 are shown in Figs. 4*b*, 5*b*, 6*b*, and 7*b*, respectively. In general, the shape of the isotherms corresponds closely to the flow structure. In all experiments, the temperature distribution is characterized by clustered vertical isotherms near the hot and cold walls and a stably stratified core in the middle of the cavity. Along the cold wall, the temperature gradients are high in the upper region and decrease toward the bottom. The opposite trend is evident at the hot wall. A plot of the local Nusselt numbers at the hot and cold walls is shown in Fig. 8 for experiment 1. At both walls, the Nusselt number is maximum where the main flow impinges. In natural convection of a high Prandtl number fluid in the same Rayleigh number range [2], this maximum is expected to be closer to the top (bottom) of the cold (hot) wall than can be seen from Fig. 8.

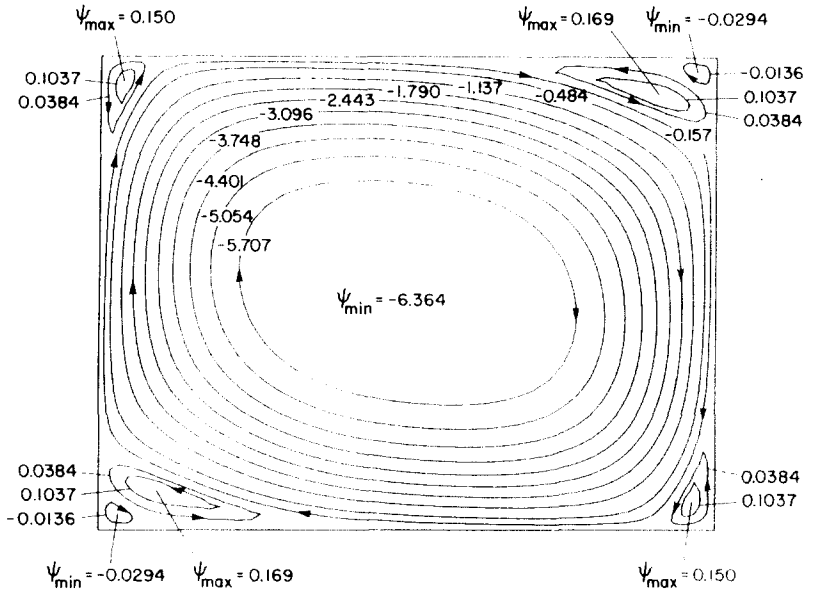

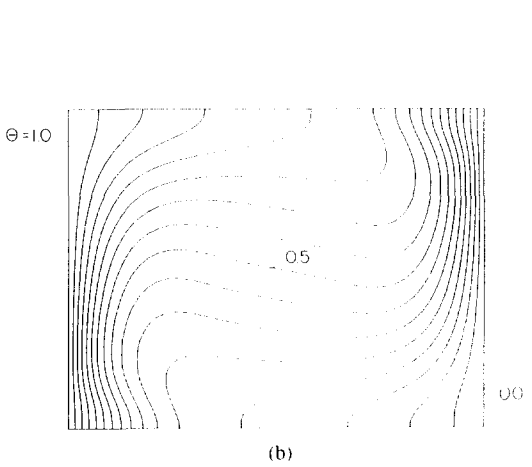

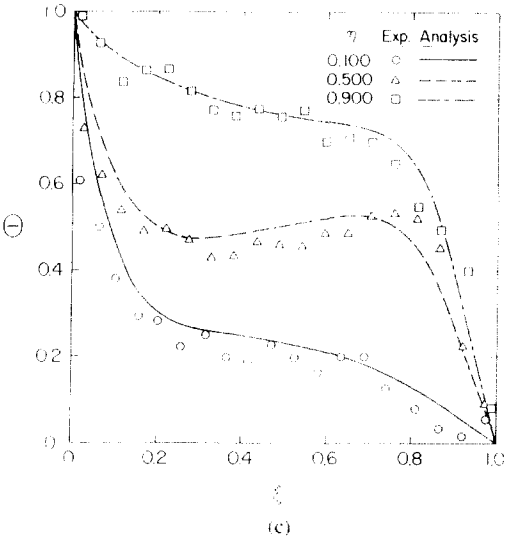

Figure 5. Measured and predicted results for experiment 2. (*a*) Streamlines; (*b*) isotherms (equal increments); (*c*) temperature profiles.

Figures 4*b* and 5*b* show the variation in the shape of the isotherms for two different aspect ratios. In the experiments with gallium (3 and 4), asymmetries about the diagonals can also be seen from the predicted isotherms (Figs. 6*b* and 7*b*). A comparison of Fig. 6*b* (Ra = 1.682×10^5) and Fig. 7*b* (Ra = 6.727×10^5) reveals the importance of the Rayleigh number to the structure of the isotherms. For increasing Rayleigh numbers, the width of the stably stratified core increases, which can be attributed to the intensification of the flow. Because of the nonuniformities in the heat exchanger temperatures in the experiments with gallium, a direct comparison of the predicted flow and heat transfer patterns for the experiments with tin (1 and 2) and with those for gallium (3 and 4) cannot be made.

Comparison of Predictions with Data

The temperature profiles measured at three different heights in the liquid tin are compared to the predictions in Figs. 4*c* and 5*c*. While there is some scatter in the data, the temperature predictions qualitatively agree with the experimental data. Some of the discrepancies may be attributed to heat losses from the test cell to the ambient as well as to measurement errors (refer to the experimental setup for tin).

The scatter in the temperature data acquired with tin may have several causes. First, the immersion of a thermocouple probe in a liquid metal undergoing natural convection is believed to cause the onset of temperature oscillations [13]. Second, the on-off control

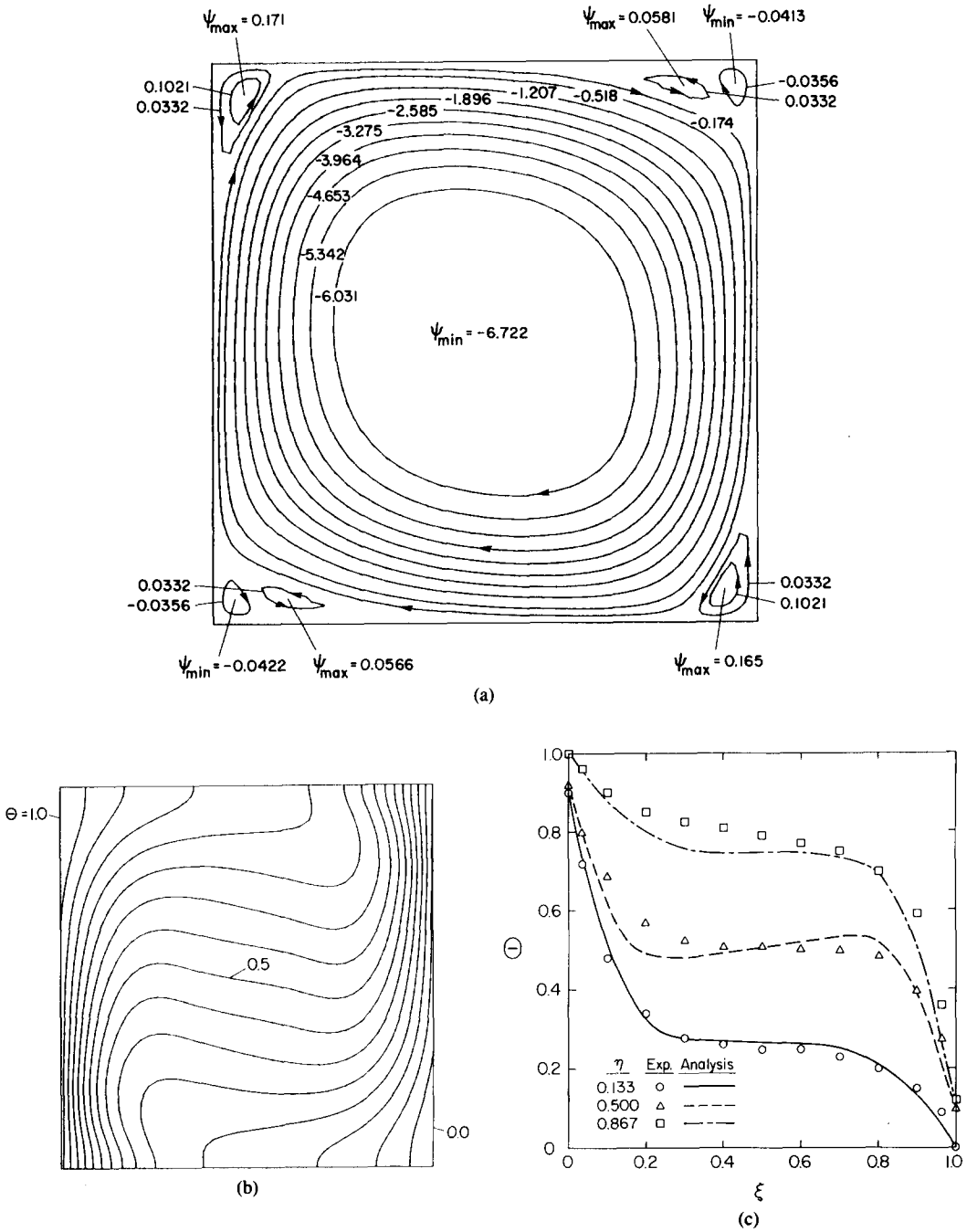

Figure 6. Measured and predicted results for experiment 3. (*a*) Streamlines; (*b*) isotherms (equal increments); (*c*) temperature profiles.

employed to achieve uniform temperatures over the heat exchanger surfaces produces an oscillation in the system. Third, the thermocouples are accurate to within only $\pm 0.1\,^{\circ}C$, while the position of the thermocouple probe is measured with an accuracy of only ± 1 mm (see above). The scatter of the data shown in Figs. 4*c* and 5*c* may be explained by these uncertainties, since the temperature difference between the hot and cold walls in the experiments with tin is only $2.5\,^{\circ}C$.

Comparisons of the measured and predicted temperature profiles for the experiments with gallium are presented in Figs. 6*c* and 7*c*. In general, the agreement between the measured and predicted temperatures is better than 5% of the temperature difference across the test cell. For both experiments (ie, 3 and 4), the results of the numerical simulations indicate stronger natural convection than was present in the experiments. This may be attributed to the presence of the thermocouple rakes in the liquid gallium, which tend to suppress the flow. In addition, three-dimensional structures in the flow [6] may influence the temperature distribution and cause some discrepancies between the measured and predicted results. The above comparisons also show that it is important to account in the simulations for the nonuniformities in the heat exchanger temperatures. The present

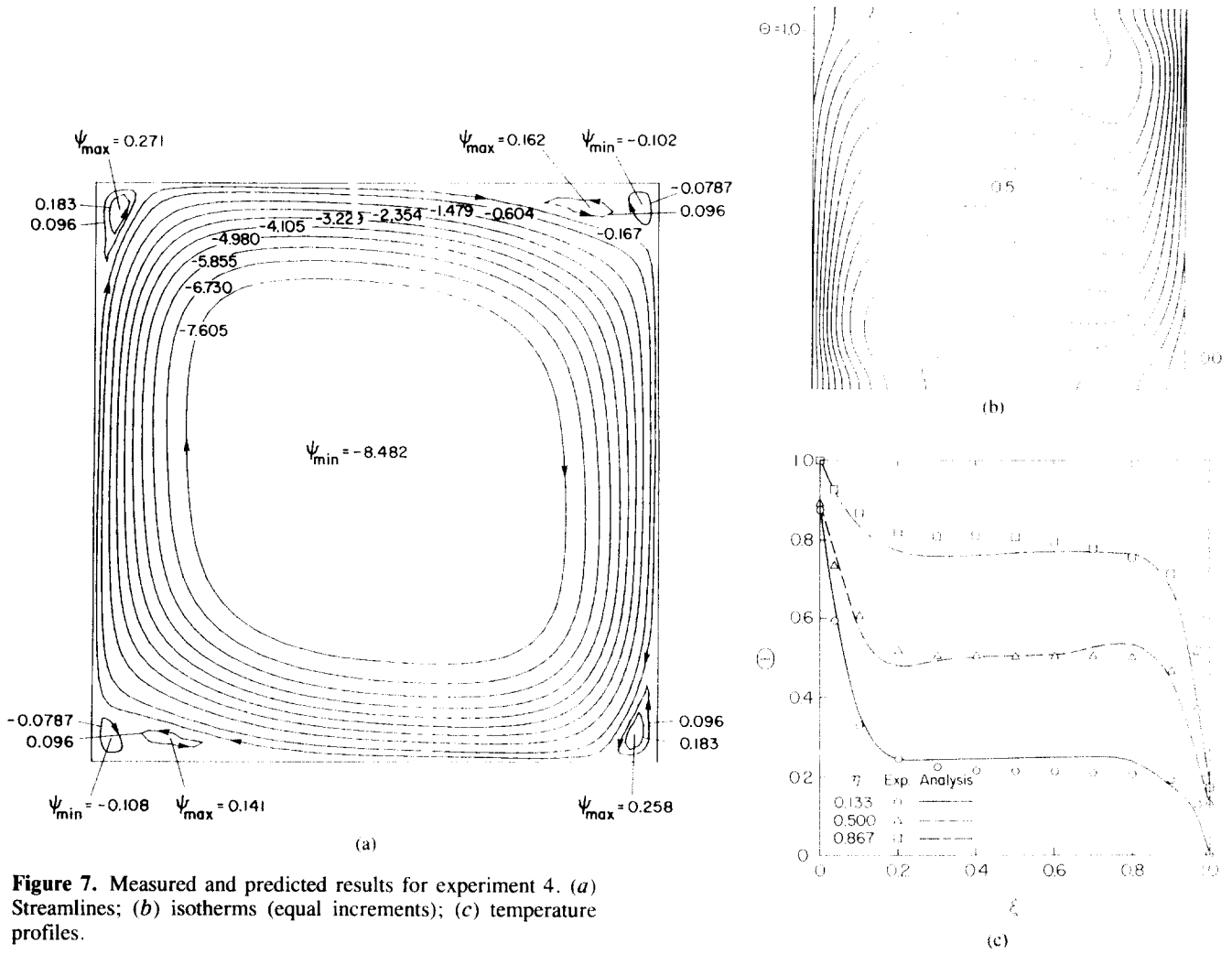

Figure 7. Measured and predicted results for experiment 4. (*a*) Streamlines; (*b*) isotherms (equal increments); (*c*) temperature profiles.

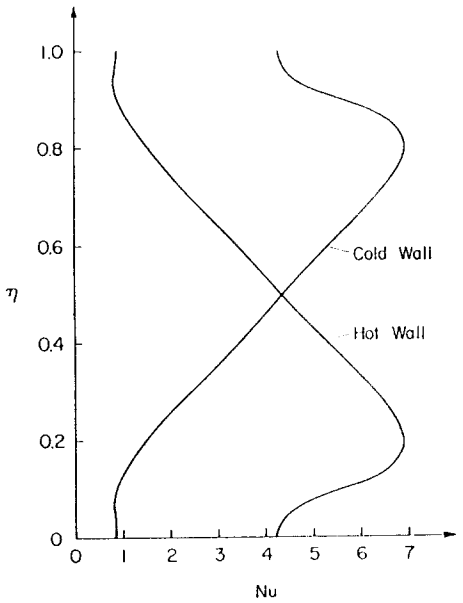

Figure 8. Variation of the local Nusselt number at the vertical walls for experiment 1.

procedure seems to produce satisfactory agreement for the temperature gradients near the vertical walls.

CONCLUSIONS

A combined experimental and numerical study is made of natural convection of liquid metals in vertical cavities. Experiments are conducted using two different test cells and two liquid metals. Temperature measurements and two-dimensional simulations of the experiments are employed to illustrate the fluid flow and heat transfer phenomena occurring in the present system. It is found that the flow is characterized by a large convection cell in the center of the cavity and smaller recirculation cells in the corners. The local heat fluxes at the hot and cold walls show a variation reflecting the flow patterns. Overall, the present results conclusively show that natural convection in liquid metals is considerably different from that in high Prandtl number fluids.

Although the agreement between the measured and predicted temperatures is relatively good, the results suggest that more accurate experimental and numerical techniques are needed to fully understand the complicated natural convection patterns in the present system. In particular, measurements of the velocity distribution in the enclosure would be highly desirable for verifying the predicted flow patterns. Attempts were made to

measure the velocity with an incorporated magnetic probe [14], but they were unsuccessful, apparently because the velocities were too small. In addition, the present results indicate the presence of three-dimensional flow structures, especially in the corners of the cavity. High-accuracy three-dimensional numerical simulations are needed to resolve these structures. However, the large number of nodal points required, together with the slow rate of convergence, may prohibit such calculations because of their high cost [6]. Finally, additional experiments should be performed, covering larger ranges of the Rayleigh number and aspect ratio.

This research was supported in part by the National Science Foundation under grant CBT-8313573. The computing facilities were made available by Purdue University Computing Center.

NOMENCLATURE

A	aspect ratio, H/L, dimensionless
g	gravitational acceleration, m/s^2
h	convective heat transfer coefficient, W/(m^2 K)
H	height of enclosure, m
k	thermal conductivity, W/(m K)
L	length of enclosure, m
Nu	Nusselt number ($=hL/k$), dimensionless
p	pressure ($=PL^2/\rho\alpha^2$), dimensionless
P	pressure, (N/m^2)
Pr	Prandtl number ($=\nu/\alpha$), dimensionless
Ra	Rayleigh number [$=g\beta(T_H - T_C)L^3/\nu\alpha$], dimensionless
T	temperature, K
$\underset{\sim}{u}$	velocity vector ($=\underset{\sim}{U}/L/\alpha$), dimensionless
$\underset{\sim}{U}$	velocity vector, m/s
x	horizontal coordinate, m
y	vertical coordinate, m

Greek Symbols

α	angular coordinate
β	coefficient of thermal expansion, 1/K
η	vertical coordinate ($=y/L$), dimensionless
Θ	temperature [$=(T - T_C)/(T_C)$], dimensionless
ν	kinematic viscosity, m^2/s
ξ	horizontal coordinate ($=x/L$), dimensionless
ρ	density, kg/m^3

Subscripts

C	cold
H	hot

REFERENCES

1. Ostrach, S., Natural Convection in Enclosures, *Advances in Heat Transfer,* Eds. J. P. Hartnett and T. F. Irvine, Jr., **8**, 161-227, Academic Press, New York, 1972.
2. Catton, I., Natural Convection in Enclosures, in *Heat Transfer 1978,* Vol. 6, pp. 13-31, Hemisphere, Washington, DC, 1978.
3. Catton, I., Bejan, A., Greif, R., and Hollands, K. G. T., Natural Convection in Enclosures, *Proceedings of a Workshop on Natural Convection,* K. T. Yang and J. R. Lloyd, Eds., pp. 24-35, University of Notre Dame, Notre Dame, IN, 1983.
4. Stewart, M. J., and Weinberg, F., Fluid Flow in Liquid Metals: 1. Theoretical Analysis, *J. Crystal Growth,* **12**, 217-227, 1971.
5. Stewart, M. J., and Weinberg, F., Fluid Flow in Liquid Metals: 2. Experimental Observations, *J. Crystal Growth,* **12**, 228-238, 1971.
6. Viskanta, R., Kim, D. M., and Gau, C., Three-Dimensional Natural Convection Heat Transfer of a Liquid Metal in Cavity, *Int. J. Heat Mass Transfer,* **29**, 475-485, 1986.
7. Harrison, C., and Weinberg, F., The Influence of Convection on Heat Transfer in Liquid Tin, *Metall. Trans. B,* **16B**, 355-357, 1985.
8. Winters, K. H., Mixed Convection of Liquid Metals in Narrow Cavities, *Liquid Metal Eng. Technol.,* 167-172, 1984.
9. Hedges, E. S., *Tin and its Alloys,* Edward Arnold, London, 1960.
10. Cubberly, W. H., *Metal Handbook, Properties and Selection: Nonferrous Alloys and Pure Metals,* 9th Ed., ASM, Metal Park, OH, 1979.
11. Patankar, S., *Numerical Heat Transfer and Fluid Flow,* Hemisphere, New York, 1980.
12. Beckermann, C., Ramadhyani, S., and Viskanta, R., Natural Convection Flow and Heat Transfer Between a Fluid Layer and a Porous Layer Inside a Rectangular Enclosure, in *Natural Convection in Porous Media,* V. Prasad and N. A. Hussain, Eds., pp. 1-12, ASME, New York, 1986.
13. MacAulay, L. C., and Weinberg, F., Liquid Metal Flow in Horizontal Rods, *Met. Trans.,* **4**, 209-2107, 1973.
14. Ricou, R., and Vives, C., Local Velocity and Mass Transfer Measurements in Molten Metals Using an Incorporated Magnetic Probe, *Int. J. Heat Mass Transfer,* **25**, 1579-1588, 1982.